

Computing the alpha complex using dual active set quadratic programming

Erik Carlsson¹ and John Carlsson²

¹Department of Mathematics, UC Davis, 1 Shields ave. Davis, CA, 95618, 530-754-0274, ecarlsson@math.ucdavis.edu

²Department of Industrial Engineering, University of Southern California, jcarlss@usc.edu,

Abstract

The alpha complex is a fundamental data structure from computational geometry, which encodes the topological type of a union of balls $B(x; r) \subset \mathbb{R}^m$ for $x \in S$, including a weighted version that allows for varying radii. It consists of the collection of “simplices” $\sigma = \{x_0, \dots, x_k\} \subset S$, which correspond to nonempty $(k + 1)$ -fold intersections of cells in a radius-restricted version of the Voronoi diagram $\text{Vor}(S, r)$. Existing algorithms for computing the alpha complex require that the points reside in low dimension because they begin by computing the entire Delaunay complex, which rapidly becomes intractable, even when the alpha complex is of a reasonable size. This paper presents a method for computing the alpha complex without computing the full Delaunay triangulation by applying Lagrangian duality, specifically an algorithm based on dual quadratic programming that seeks to rule simplices out rather than ruling them in.

1 Introduction

Given a point cloud and a threshold radius, the alpha complex is a simplicial complex whose simplices correspond to relationships between points that are relevant in the sense that they are not too far apart. It is a generalization of the Delaunay triangulation, another fundamental computational geometric structure, which is the dual graph of the Voronoi diagram. Alpha complexes are used in a diverse range of application areas to study the shape of datasets, such as molecular biology [30], crystallography [37], shape reconstruction [13], and persistent homology [33].

Formally, let $S = \{x_1, \dots, x_N\} \subset \mathbb{R}^m$ be a set of points, and let $r \geq 0$ be a nonnegative real number. The *radius-restricted Voronoi diagram* is the

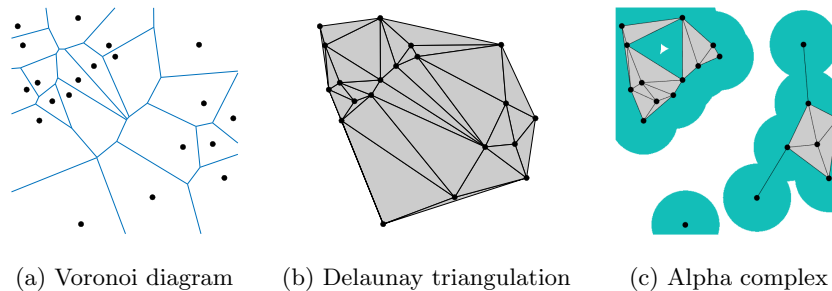


Figure 1: The Voronoi partition associated with a set of points (1a), and the Delaunay triangulation (1b). The alpha complex (1c) is a subset of the Delaunay triangulation in which one removes simplices (which in the plane simply correspond to points, edges, and triangles) that violate the distance property that $V_x(r) \neq \emptyset$.

collection

$$\text{Vor}(S, r) = \{V_x(r) : x \in S\},$$

where $V_x(r) = V_x \cap B(x; r) \subset \mathbb{R}^m$ is intersection of the usual Voronoi cell

$$V_x = \{y \in \mathbb{R}^m : \|y - x\| \leq \|y - x'\| \forall x' \in S\}$$

with the ball $B(x; r)$ of radius r centered about x . The alpha complex is the *nerve* of $\text{Vor}(S, r)$, that is, the simplicial complex defined as the collection

$$\text{Alpha}(S, r) = \left\{ \sigma \subset S : \bigcap_{x \in \sigma} V_x(r) \neq \emptyset \right\}.$$

Simply put, a subset $\sigma = \{x_{i_0}, \dots, x_{i_k}\} \subset S$ belongs to $\text{Alpha}(S, r)$ if there exists a point $y \in \mathbb{R}^m$ that is equidistant from every member of σ , i.e. $\rho := \|y - x_{i_0}\| = \dots = \|y - x_{i_k}\| \leq r$, and furthermore, $\|y - x\| \geq \rho$ for all $x \in S$. A given subset σ of size $k + 1$ is called a k -dimensional simplex of $\text{Alpha}(S, r)$. The alpha complex is a subcomplex of $\text{Delaunay}(S)$, which is the nerve of the full Voronoi diagram $\text{Vor}(S)$, and which agrees with the Delaunay triangulation when the points of S are planar points in general position. Figure 1 shows one of these constructions.

More generally, there exists an extension of the alpha complex known as the weighted alpha complex, in which the Voronoi cells are replaced by a power diagram, which allows for balls of different radii. An example of a power diagram and its associated weighted alpha complex is shown in Figure 2 below. The weighted alpha complex gives rise to the *alpha shapes* [19], whose applications include the aforementioned study of biomolecules. A further extension is the wrap complex, which is used in surface modeling [20, 6].

In terms of computational topology, the alpha complex is homotopy equiv-

alent to the union of the cells

$$A = \bigcup_{x \in S} V_x(r) = \bigcup_{x \in S} B(x; r) \subset \mathbb{R}^m.$$

It can therefore be used to compute the topological type of a space which can be covered by balls from the combinatorial data of which cells intersect nontrivially. This is also true of the the *Čech complex* $\check{\text{Cech}}(S, r)$, defined as the nerve of the covering by the balls as on the right, which satisfies

$$H_*(\text{Alpha}(S, r)) \cong H_*(\check{\text{Cech}}(S, r)),$$

both sides being isomorphic to $H_*(A)$. The alpha complex is by definition a subcomplex of the Čech complex $\text{Alpha}(S, r) \subset \check{\text{Cech}}(S, r)$, and it typically has far fewer simplices. This is advantageous, for instance, for computing *persistent homology* [16, 44], noting both the Čech and alpha complexes give rise to a family of complexes, which are “filtered” by varying the radius r .

Perhaps the most common construction for computing persistent homology is the Vietoris-Rips construction [24], especially through a highly efficient open source software tool known as Ripser [5]. Čech and alpha complexes can also be used for this purpose and have advantages over Vietoris-Rips in that they typically have far fewer simplices. Moreover, because of theoretical guarantees stemming from the nerve theorem, their homology groups may be calculated exactly from usual, non-persistent homology, which requires only Gaussian elimination. One reason Čech and alpha complexes are not as commonly used is that Vietoris-Rips allows for non-Euclidean metrics, but a more crucial reason is the poor scalability of the Delaunay construction in dimensions greater than three.

Most methods for computing the alpha complex begin by computing the full Delaunay complex, and removing simplices which do not come from a Voronoi face which has the restricted radius property [12, 19, 17, 39]. There are a wide range of highly efficient algorithms for computing the Delaunay complex in dimensions $m \leq 3$, many of which exploit the empty circumsphere property, which states that a 3-simplex tetrahedron belongs to $\text{Delaunay}(S)$ in \mathbb{R}^3 if and only if its circumsphere contains no points [8, 25, 3, 26, 9, 43]. In dimension $m > 3$, one can still compute $\text{Delaunay}(S)$ by applying flipping methods [18], or by reducing the problem to finding a convex hull in \mathbb{R}^{m+1} as in [22]. In terms of computing persistent homology, other authors have a combination of the alpha complex and the Vietoris-Rips construction to incorporate to improve efficiency [32].

In higher dimensions, it is often the case that the alpha complex has a reasonable number of simplices, but the full Delaunay complex is far too large to be computed, having on the order of $O(N^{\lceil m/2 \rceil})$ simplices. In this situation, the general pipeline of the previous paragraph must be replaced by one that does not compute the full complex. One algorithm that takes this into account is given in [34], whose complexity depends on the total size of the output, and on bounds relating the pairwise distance between points and the upper bound on the radius r . As an additional reduction, one is often only interested in subcomplex $\text{Alpha}_{\leq d}(S, r)$ consisting of simplices of dimension at most d .

A brute-force approach would be to formulate the existence of each individual simplex $\sigma \in \text{Alpha}(S, r)$ as an optimization problem

$$\begin{aligned} & \underset{y \in \mathbb{R}^m}{\text{minimize}} && \|y - x\|^2 \\ & \text{subject to} && \|y - x_i\| \leq \|y - x_j\| \quad x_i \in \sigma, x_j \in S - \sigma, \\ & && \|y - x_i\| = \|y - x_j\| \quad x_i, x_j \in \sigma, i \neq j \end{aligned} \tag{1}$$

where x is any particular element of σ , all choices yielding the same result. Specifically, we can conclude that a given simplex σ is in $\text{Alpha}(S, r)$ when the constraints are feasible, and the minimizing value is at most r^2 . By squaring the conditions, expanding and canceling terms, we actually see that the above inequalities and equalities are in just linear constraints, making (1) into a constrained (convex) quadratic program.

Computing $\text{Alpha}_{\leq d}(S, r)$ would thus require solving

$$\binom{N}{1} + \dots + \binom{N}{d+1}$$

such quadratic programs. In reality, many of these simplices may be ruled out, including any simplex σ which is not an element of the Čech complex, or one whose faces have been determined not to exist, assuming we are proceeding in order of increasing dimension. Additionally, we only need to consider those constraints in (1) coming from vertices x_j which are neighbors in the one-skeleton of $\check{C}ech(S, r)$. Despite these reductions, computing the alpha complex directly is too burdensome to be practical for large values of N to be of practical value.

The point of this paper is to show that that this approach becomes practical, provided that we use Lagrangian duality to solve (1) instead of directly attacking the original primal problem. The fact that any feasible point in the dual problem determines a lower bound for the optimum of the primal problem is well-suited for this purpose because it allows the algorithm to terminate whenever a dual feasible point is found with an objective value greater than r^2 , which in many cases will happen at an early stage. Furthermore, the form of this particular dual problem, shown in (10), has the property that the zero vector $\lambda = 0$ is always feasible. Thus, there is no startup cost associated with identifying an initial feasible solution. Another crucial benefit is that while the size of the alpha complex is related to the rough dimension of the space traversed by the point cloud S , there is essentially no dependence on the embedding, because dual programming algorithms depend only on the respective dot products.

Our method, which is straightforward to describe, is implemented for the more general weighted alpha complex, and is described in Algorithm 1 below. Beyond using dual programming as described, we have taken advantage of one further observation: the minimization problem (1) for a given face is the same for that of the full cell V_x , except that those inequalities determined by faces are replaced by the corresponding equalities. The main loop of Algorithm 1 is written in a way so that the coefficients are only calculated once per vertex, rather than once per potential simplex, which would otherwise be a

major computational cost. Algorithm 1 was written in MAPLE, and is available at the first author’s webpage: <https://www.math.ucdavis.edu/~ecarlsson/>. This includes an implementation of an elegant recent dual active set method due to [2], which we used to solve the dual quadratic programs.

In Section 4, we illustrate our algorithm in several examples which we validated using homology calculations, and which are also available online as MAPLE worksheets. We compared our answer against the output of persistence calculations which we carried out in Ripser. In some of those example there appears to be a potential computational advantage to using the alpha complex via our algorithm, as there often is for existing algorithms for the alpha complex in two or three dimensions [36]. However, the goal in comparing those answers is not to show a speed boost in persistent homology calculations, but rather to give a rigorous test of the correctness of the algorithm, which would fail to capture the correct homology if even a single simplex is incorrect. We make no comparison of the running time of our homology calculations, for which we used a general sparse matrix rank algorithm due to Dumas and Villard [15] instead of specialized methods. Intuitively, homology and persistent homology calculations of alpha complexes are expected to be faster than Vietoris-Rips calculations once the alpha complex has been computed, as the former is a subcomplex of the latter.

As we described above, the alpha complex has far reaching applications beyond persistent homology computations, firstly in that it produces concrete geometric models, which give rise to the alpha shapes. In terms of homology, it is also useful that the alpha complex provides exact answers rather than persistence diagrams, which we use in Section 4.5 to carry out an interesting calculation from geometric representation theory. Another recent application is due to the present authors, who discovered a hidden family of alpha complexes associated to the super-level sets of an arbitrary kernel density estimator in [10]. Implementing this construction in way that does not scale poorly with the embedding dimension was the motivation behind our main algorithm.

1.1 Acknowledgments

Both authors were supported by the Office of Naval Research (ONR) N00014-20-S-B001 during this project, which they gratefully acknowledge.

2 Preliminaries on computational topology

We set some notation and background about filtered simplicial complexes, referring to [21] for more details.

2.1 Computational topology

Let S be a set of size N , which we assume is totally ordered.

Definition 1. A simplicial complex X on a vertex set S is a collection of nonempty subsets of S which is closed under taking nonempty subsets.

The elements of X are called simplices, and are denoted $\sigma = [\sigma_0, \dots, \sigma_k]$, using closed brackets to indicate that the elements are distinct and written in order. The number k is called the dimension of σ , and the set of simplices of dimension k is denoted X_k . If $\sigma \in X$ is a simplex, then the subsets for which $\sigma' \subset \sigma$ are called the faces of σ . The collection of simplices of dimension at most k is a subcomplex called the k -skeleton of X , which is denoted $\text{Skel}_k(X)$. For instance, $\text{Skel}_1(X)$ is a complex with only zero and one-dimensional simplices, which is the same data as a graph.

The following definition will also appear in Algorithm 1 below.

Definition 2. Let X be a complex. We define $\text{Lazy}_k(X)$ to be the largest simplicial complex Z on the vertex set S for which $\text{Skel}_k(Z) = \text{Skel}_k(X)$.

For instance, we have that $\text{Lazy}_{-1}(X)$ is the complete complex on the vertex set S , whereas $\text{Lazy}_0(X)$ is similar, but contains only those vertices which are in X_0 , which need not be all of S . The one-dimensional lazy construction $\text{Lazy}_1(X)$ appears in the definition of the Vietoris-Rips and lazy Witness complexes [14, 24, 35], which are widely used to compute persistent homology.

Definition 3. The Barycentric subdivision $\text{Sd}(X)$ is the complex whose vertices are the simplices in X , and whose k -simplices consist of strictly increasing flags $\sigma^{(0)} \subset \dots \subset \sigma^{(k)}$ of elements of X .

Definition 4. If the vertex set S is equipped with a map to \mathbb{R}^m , then the geometric realization is defined by

$$|X| = \bigcup_{\sigma \in X} \text{conv}(\sigma) \subset \mathbb{R}^m \quad (2)$$

where $\text{conv}(\sigma)$ is the convex hull of the images of the vertices. If no such map is given, the geometric realization is defined to be the standard one in which the i th element of S is sent to the unit vector $e_i \in \mathbb{R}^N$.

Combining the two definitions, we see that a function $\Phi : X \rightarrow \mathbb{R}^m$ determines a linear map $|\text{Sd}(X)| \rightarrow \mathbb{R}^m$.

In persistent homology, one is interested in a nested family of complexes, depending on a real parameter a :

Definition 5. A filtered complex is a pair (X, w) consisting of a simplicial complex X , and a weight function $w : X \rightarrow \mathbb{R}$, which has the property that the subset $X(a) = w^{-1}(-\infty, a] \subset X$ is a complex for every a .

The data of a pair (X, w) and the corresponding nested collection of filtered complexes $X(a)$ are interchangeable. If X is filtered by w , then there are induced filtrations on $X(a)$, $\text{Skel}_k(X)$, and $\text{Lazy}_k(X)$. The filtration on $\text{Lazy}_k(X)$ is the one for which $w(\sigma)$ is the max of $w(\sigma')$ as σ' ranges over all elements of $\text{Skel}_k(X)$ which are faces of σ . The first two are simply by restriction.

If X is a complex then the chain group is the vector space of all formal linear combinations

$$C_k = \left\{ \sum_{\sigma \in X_k} c_\sigma \sigma \right\} \quad (3)$$

where we will always take coefficients to be elements of a finite field $c_\sigma \in \mathbb{F}_p$ for p a prime. The k th homology group is given by

$$H_k(X, \mathbb{F}_p) = Z_k / B_k = \ker \partial_k / \text{Im } \partial_{k+1} \quad (4)$$

where $\partial_k : C_k \rightarrow C_{k-1}$ is defined on each basis vector $\sigma = [x_0, \dots, x_k]$ by

$$\partial_k(\sigma) = \sum_{i=0}^k (-1)^i [x_0, \dots, \widehat{x}_i, \dots, x_k]$$

The k th Betti number $\beta_k(X, \mathbb{F}_p)$ is the dimension of $H_k(X, \mathbb{F}_p)$.

Filtered complexes have the additional structure of persistent homology groups, which assemble the individual homology groups $H_k(X(a))$ for each value of a into a family of filtered homology groups. Instead of individual Betti numbers, one has a collection of persistence intervals often called a barcode diagram, such as the Ripser outputs shown in Section 4. Roughly speaking, one can infer the Betti numbers of a point cloud by counting the significant intervals in that diagram. For an introduction to persistent homology, we refer to [21].

2.2 The Nerve theorem

Let $\mathcal{U} = \{U_x : x \in S\}$ be a collection of subsets of \mathbb{R}^m with index set S .

Definition 6. The Čech nerve, written $\text{Nrv}(\mathcal{U})$, is the complex with vertex set S , and for which

$$[x_0, \dots, x_k] \in X \iff U_{x_0} \cap \dots \cap U_{x_k} \neq \emptyset \quad (5)$$

Then the classical nerve theorem of Leray [29] states:

Theorem 1 (Leray). *Suppose that \mathcal{U} has the property that any k -fold intersection of the U_x is contractible (which occurs, for instance, if every U_x is convex). Then $\text{Nrv}(\mathcal{U})$ is homotopy equivalent to the union $\bigcup \mathcal{U} \subset \mathbb{R}^m$.*

In some cases, the nerve equivalence has an explicit form. If \mathcal{U} is a covering by balls, then the linear map $|\text{Nrv}(\mathcal{U})| \rightarrow \bigcup \mathcal{U}$ determined by sending each vertex to the corresponding center induces the nerve equivalence. More generally, if every U_x is convex, and we select any representatives $x_\sigma \in U_{\sigma_0} \cap \dots \cap U_{\sigma_k}$, we have an induced map $\Phi : |\text{Sd}(X)| \rightarrow \bigcup \mathcal{U}$, which also induces the nerve equivalence via the equivalence of $|X|$ with the subdivision $|\text{Sd}(X)|$. See [7] for a proof, and more on the general setup of nerve theorems.

2.3 Power diagrams

Suppose that $S \subset \mathbb{R}^m$, and let $p : S \rightarrow \mathbb{R}$ be a function, called the weight map. We now have a function $\pi : \mathbb{R}^m \rightarrow \mathbb{R}$ given by

$$\pi(y) = \min_{x \in S} \pi_x(y), \quad \pi_x(y) = \|y - x\|^2 - p(x). \quad (6)$$

Definition 7. Let S, p be as above and let $a \in \mathbb{R}$. Then the weighted ball cover denoted $\mathcal{U} = \text{PowCov}(S, p, a)$ is given by $\mathcal{U} = \{U_x : x \in S\}$, where

$$U_x = \{y \in \mathbb{R}^m : \pi_x(y) \leq a\} \quad (7)$$

is either a closed ball, or is empty.

Definition 8. The weighted power diagram is the covering $\text{PowDiag}(S, p, a) = \{U_x \cap V_x : x \in S\}$ where

$$V_x = \{y : \pi_x(y) \leq \pi_{x'}(y) \text{ for all } x' \in S\}, \quad (8)$$

and $U_x \in \text{PowCov}(S, p, a)$ ranges over the corresponding elements in the weighted ball cover.

The Čech and alpha complexes are the filtered complexes which are the nerves of the weighted ball and power cover, respectively:

Definition 9. The Čech complex denoted $(X, w) = \check{\text{Cech}}(S, p)$ is the filtered complex determined by $X(a) = \text{Nrv}(\text{PowCov}(S, p, a))$. We let $\check{\text{Cech}}(S, p, a_1)$ be the filtered subcomplex $X(a_1)$ which is cut off at weight a_1 .

Definition 10. The weighted alpha complex $(X, w) = \text{Alpha}(S, p)$ is the filtered complex for which $X(a) = \text{Nrv}(\text{PowDiag}(S, p, a))$, with a similar definition of $\text{Alpha}(S, p, a_1)$.

Said another way, we have a simplex $\sigma = [x_0, \dots, x_k] \in X(a)$ if the weighted Voronoi face $V_\sigma = V_{\sigma_0} \cap \dots \cap V_{\sigma_k}$ is nonempty, and there exists a point $x \in V_\sigma$ satisfying $\pi_{x_i}(x) \leq a$ for any i , noticing that the π_{x_i} all become equal when restricted to V_σ . Adopting the terminology of the witness complex, such a point x is called a *witness* for σ because its existence determines that $\sigma \in X(a)$. Since π_{x_i} is a quadratic function and V_σ is convex, we have a unique minimizer x_σ for every $\sigma \in X(a)$. The collection of these points is described as a map:

Definition 11. Let $X = \text{Alpha}(S, p)$. The *witness map* is the function $\Phi : X \rightarrow \mathbb{R}^m$ which carries each simplex $\sigma = [x_0, \dots, x_k]$ to the unique element $x_\sigma \in V_\sigma$ that minimizes $\pi_{x_j}(x)$, which is independent of the choice of j .

In particular, by restricting by to $X(a)$, we obtain a linear map

$$|\text{Sd}(X(a))| \rightarrow \bigcup \text{PowDiag}(S, p, a)$$

by the discussion in Section 2.2. An example of a power diagram, its alpha complex, and the associated witness map is shown in Figure 2.

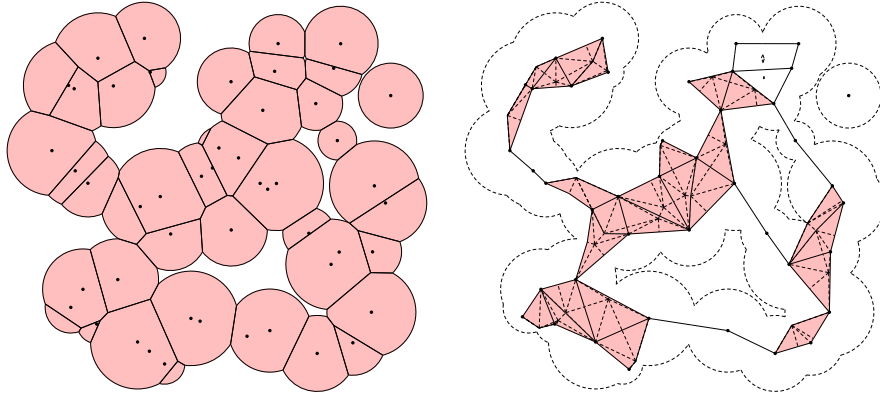


Figure 2: On the left, a randomly generated power diagram in the plane, cut off at some weight a . On the right, the Barycentric subdivision of its associated alpha complex mapped into \mathbb{R}^2 using the witness map Φ , which induces the nerve isomorphism.

The usual (unweighted) alpha complex and Voronoi diagram from the introduction are given by

$$\text{Alpha}(S, r) = \text{Alpha}(S, p, r^2), \quad \text{Vor}(S, r) = \text{PowDiag}(S, p, r^2)$$

in which $p(x) = 0$ for all x . Notice that the full vertex set for $X = \text{Alpha}(S, r)$ is given by $X_0(a) = S$ for $a \geq 0$, and is empty for $a < 0$, whereas the vertices appear at different times in the weighted case.

3 Algorithm for computing the alpha complex

We recall some facts about dual quadratic programming, and present our main algorithm.

3.1 Dual programming

Let A be an $n \times m$ matrix, writing A_i for the i th row. Let $V \in \mathbb{R}^n$, $x_0 \in \mathbb{R}^m$, and let $J \subset \{1, \dots, n\}$ be a subset. Let $(y^*, c^*) = \text{PrimalQP}(x, A, V, J)$ be the optimal solution and objective value to the quadratic program

$$\begin{aligned} & \underset{y \in \mathbb{R}^m}{\text{minimize}} && \frac{1}{2} \|y - x\|^2 \\ & \text{subject to} && A_i y = V_i, \quad i \in J, \\ & && A_i y \leq V_i, \quad i \notin J \end{aligned} \tag{9}$$

To indicate that there is no feasible solution, the routine will return $c^* = \infty$, and an arbitrary value of x^* .

The dual quadratic program is

$$\begin{aligned} & \underset{\lambda \in \mathbb{R}^n}{\text{maximize}} && -\frac{1}{2}\lambda^t B \lambda + U^t \lambda \\ & \text{subject to} && \lambda_i \geq 0, \quad i \notin J \end{aligned} \tag{10}$$

where

$$B = AA^t, \quad U = Ax - V. \tag{11}$$

We will denote its solution by $(\lambda^*, c^*) = \text{DualQP}(B, U, J, c_1)$, where c_1 is an upper bound on the allowable value of c^* . If we find that $c^* > c_1$, then the algorithm will terminate early and return $c^* = \infty$, together with an arbitrary value λ^* . If an optimum is obtained, the minimizing solution of the primal QP is determined by the KKT conditions, and is given by

$$y^* = x - A^t \lambda^*. \tag{12}$$

Example 1. For every feasible point of (10), weak duality states that the corresponding value of the objective function is a lower bound on the solution in (9). Suppose for some i we have that $A_i x < V_i$, meaning that x is not on the feasible side in (9). Then the minimizer of (10) along the line $\lambda_i = t$ and all other λ_j are zero occurs at $t = U_i/B_{i,i}$. Substituting this into (10) gives

$$-\frac{1}{2}B_{i,i}t^2 + U_i t = \frac{U_i^2}{2B_{i,i}} = \frac{(A_i x - V)^2}{2\|A_i\|^2},$$

which is the lower bound corresponding to the point on the plane $A_i y = V$ which is as close as possible to x .

To solve (10), we have incorporated a compiled MAPLE implementation of a highly efficient and elegant recent active set method due to [2].

3.2 The alpha complex as a quadratic program

Consider the filtered alpha complex $X = \text{Alpha}(S, p, a_1)$ for $S \subset \mathbb{R}^m$, and let $w : X \rightarrow \mathbb{R}$ be the weight map. Let $\sigma = [x_0, \dots, x_k] \subset S$ be a subset which may or may not define a simplex in X , and select any particular vertex, say $x = x_0$. Then the problem of determining whether σ determines a simplex in X amounts to solving the following constrained quadratic optimization problem:

$$\begin{aligned} & \underset{y \in \mathbb{R}^m}{\text{minimize}} && \pi_x(y) \\ & \text{subject to} && \pi_x(y) = \pi_z(y), \quad z \in \sigma - \{x\}, \\ & && \pi_x(y) \leq \pi_z(y), \quad z \in S - \sigma \end{aligned} \tag{13}$$

Specifically, we have a simplex $\sigma \in X$ if and only if (13) is feasible and the optimal solution a^* satisfies $a^* \leq a_1$. By convexity, if the problem is feasible, then there is a unique minimizer y^* with corresponding objective value a^* , and we have $w(\sigma) = a^*$, and $\Phi(\sigma) = y^*$.

This can be formulated in terms of (9). Let us write $S - \{x\} = \{x_1, \dots, x_n\}$, and let $J = \{j_1, \dots, j_k\}$ be those labels so that $\sigma - \{x\} = \{x_{j_1}, \dots, x_{j_k}\}$. The constraints may be written as

$$A_i = (x_i - x)^t, \quad V_i = \frac{1}{2} (\|x_i\|^2 - \|x\|^2 - p(x_i) + p(x))$$

for $i \in \{1, \dots, n\}$. Using (11), the dual problem is determined by

$$B_{i,j} = (x_i - x)^t (x_j - x), \quad U_i = \frac{1}{2} (p(x_i) - p(x) - \|x_i - x\|^2).$$

Thus, if we set $(\lambda^*, c^*) = \text{DualQP}(B, U, J, c_1)$ for $c_1 = (a_1 + p(x))/2$, then σ determines a simplex if $c^* \leq c_1$, and its weight is given by $w(\sigma) = 2c^* - p(x)$. The witness is given by $\Phi(\sigma) = y^*$, where by the KKT conditions (12) we have

$$y^* = x - \sum_i \lambda_i^* (x_i - x).$$

3.3 Description of the main algorithm

We present our main algorithm which computes the weighted alpha complex using dual programming. Specifically, the input consists of the data of a power diagram (S, p, a_1) as in Section 2.3, together with a nonnegative integer $d \geq 0$. The output is the d -skeleton $X = \text{Skel}_d(\text{Alpha}(S, p, a_1))$, which contains the simplices of the alpha complex up to dimension d , as well as the associated witness map $\Phi : X \rightarrow \mathbb{R}^m$. We now describe the procedure.

As a preprocessing step, we begin by computing the Čech graph G of the weighted ball cover $\text{PowCov}(S, p, a_1) = \{U_x : x \in S\}$, which is the one-skeleton of the Čech complex $\check{\text{Cech}}(S, p, a_1)$. In other words, G is the graph whose vertices are those elements $x \in S$ for which U_x is nonempty, i.e. $-p(x) \leq a_1$, and which has an edge connecting x to y if $U_x \cap U_y \neq \emptyset$. This is important for efficiency for the following reason: let $x \in S$ and suppose $S' = \{x\} \cup N_G(x) \subset S$ contains x and its neighbors in G . Then any face V_σ of $V_x \in \text{PowDiag}(S, p, a_1)$ is nonempty if and only if the corresponding face is nonempty in $\text{PowDiag}(S', p, a_1)$. This reduces the number of inequalities that need to be considered to only the necessary ones.

We then proceed to compute the alpha complex, beginning with the zero simplices, and work upwards until we reach dimension d . For each dimension $k \leq d$, we assume we have already computed the simplices of dimension up to $k - 1$, described by a $(k - 1)$ -dimensional complex X , starting with the empty complex. At step k , the algorithm may be described as follows.

1. Compute the set Σ_k consisting of all potential simplices to be tested according to the following cases:
 - (a) If $k = 0$, then Σ_k corresponds to the vertices of G . In other words, it is the set of simplices $[x]$ where $x \in S$ satisfies $-p(x) \leq a_1$.
 - (b) If $k = 1$, then Σ_k is the set of edges of G .
 - (c) If $k \geq 2$, then Σ_k is the set of k -dimensional simplices in the lazy construction, $\Sigma_k = (\text{Lazy}_{k-1}(X))_k$.
2. For each $x \in S$, do the following:
 - (a) Let $S' = \{x, x_1, \dots, x_n\}$ consist of x together with its neighbors in G . Determine the coefficients (B, U, c_1) for the dual program that describes the cell $V_x \in \text{PowDiag}(S', p, a_1)$ as in Section 3.1. The equations defining every face of V_x have the same coefficients, but with different sets J that label the equality constraints.
 - (b) For every potential face V_σ for $\sigma = [x, x_{j_1}, \dots, x_{j_k}] \in \Sigma_k$, do the following, noting that we are only considering simplices $x \leq x_{j_1} \leq \dots \leq x_{j_k}$, as the other orders have already been encountered:
 - i. Let $J = \{j_1, \dots, j_k\}$ be the indices of the equality constraints which determine the face V_σ . Solve the corresponding quadratic program using a dual active set method such as [2], terminating early if the upper bound c_1 is exceeded.
 - ii. If the quadratic program is feasible and the optimal value satisfies $c^* \leq c$, then add the simplex σ to X_k with the desired weight $w(\sigma)$ as determined by c^* . Compute the corresponding minimizer x^* using the KKT equations, and update the witness map by setting $\Phi(\sigma) = x^*$.

By using a dual active set method in step 2(b)i, we can often rule out a potential simplex using a small subset of points, as shown in Figure 3, rather than all N of them. The process of solving problem (10) involves sequentially inserting and removing iterates λ_i , which are dual variables corresponding to the data points x_i , and this insertion and removal is equivalent to efficiently selecting a (typically small) subset of data points whose existence rules out a potential simplex. The psuedo-code for this algorithm is given in Algorithm 1.

We summarize the above discussion in a proposition, which is evident:

Proposition 1. *Algorithm 1 computes the alpha complex.*

4 Examples and Applications

We illustrate Algorithm 1 in several examples. In the first, we apply the complex to a standard three-dimensional mesh generation example. We find that Algorithm 1 is not as fast as existing methods that are specialized to three

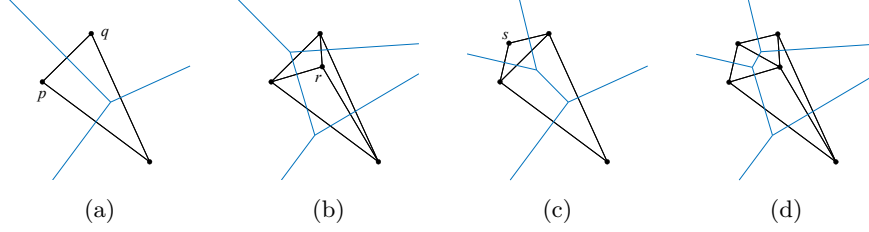


Figure 3: The Delaunay triangulation (and Voronoi diagram) for three points is shown in 3a. The segment connecting points p and q continues to be present when points r and s are inserted individually as in 3b and 3c, but vanishes when both are inserted simultaneously as in 3d. The key observation is that the simplex $[p, q]$ can be ruled out due to the “active set” $\{r, s\}$, irrespective of whatever other data points remain elsewhere in the point set.

Algorithm 1 Compute the d -skeleton of $\text{Alpha}(S, p, a_1)$

Input	$S \subset \mathbb{R}^m$ $p : S \rightarrow \mathbb{R}$ $a_1 \in \mathbb{R}$ $d \geq 0$	Vertices of the power diagram Power function Maximum allowable power Dimension of output
Output	$X \subset \mathcal{P}(S)$ $w : X \rightarrow (-\infty, a_1]$ $\Phi : X \rightarrow \mathbb{R}^m$	d -skeleton of $\text{Alpha}(S, p, a_1)$ Weight function Table of representatives
1:	$Y \leftarrow \text{Skel}_1(\check{\text{Cech}}(S, p, a_1))$	
2:	$G \leftarrow \text{Graph}(Y)$	▷ Underlying graph
3:	$X \leftarrow \emptyset$	
4:	for k from 0 to d do	
5:	if $k \leq 1$ then	
6:	$\Sigma_k \leftarrow Y_k$	
7:	else	
8:	$\Sigma_k \leftarrow (\text{Lazy}_{k-1}(X))_k$	▷ All potential k -simplices
9:	for $x \in S$ do	
10:	$\{x_1, \dots, x_n\} \leftarrow N_G(x)$	▷ Neighbors to x
11:	$B \leftarrow ((x_i - x)^t(x_j - x))_{i,j=1}^n$	
12:	$U \leftarrow \frac{1}{2}(p(x_i) - p(x) - \ x_i - x\ ^2)_{i=1}^n$	
13:	$c_1 \leftarrow (a_1 + p(x))/2$	
14:	for $\sigma = [x, x_{j_1}, \dots, x_{j_k}] \in \Sigma_k$ do	
15:	$J \leftarrow \{j_1, \dots, j_k\}$	▷ The equality constraints
16:	$(\lambda^*, c^*) \leftarrow \text{DualQP}(B, U, J, c_1)$	
17:	if $c^* \leq c_1$ then	
18:	$X \leftarrow X \cup \{\sigma\}$	
19:	$w(\sigma) \leftarrow 2c^* - p(x)$	
20:	$\Phi(\sigma) \leftarrow x - \sum_{j=1}^n \lambda_j^*(x_j - x)$	▷ KKT conditions

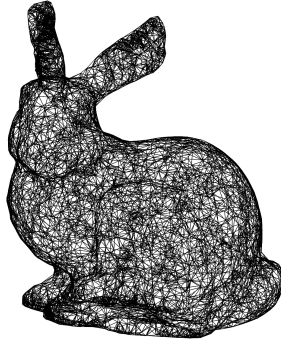


Figure 4: Alpha complex of a Stanford bunny data set with 5000 sites.

dimensions. In the second, we generate 1000 random points in \mathbb{R}^{10} and compute the alpha complex up to the three-dimensional simplices with a relatively large radius. In contrast with the three-dimensional example, this could not be done by computing the full Delaunay triangulation.

In the last two examples, we use the alpha complex to compute the homology of some interesting topological spaces from a sampling of landmark points. While the main loop of Algorithm 1 can be done in full parallel, we have not used any parallelism in our computations. The homology groups calculated below were done using a MAPLE implementation of an algorithm of Dumas and Villard [15] for computing the ranks of sparse matrices mod p . For comparison, we also compute the persistence homology groups using Ripser.

4.1 Three-dimensional mesh generation

We first apply Algorithm 1 to triangulating a three dimensional data set consisting of 5000 points sampled from surface of the Stanford bunny [40], downloaded from the CGAL website [38]. We chose a radius size of approximately 1/15 of the diameter, which led to a Čech graph with a maximum vertex degree of 200 in the graph of line 2. The resulting alpha complex, whose one-skeleton is shown in Figure 4, had sizes of $(|X_k|)_{k=0}^3 = (5000, 23830, 29995, 11163)$ simplices in each dimension. The full computation took approximately 12 seconds. This would be faster to compute using either specialized methods for three-dimensions, or using Delaunay software such as qhull [4]. Notice that the Euler characteristic gives the value of 2, indicating that the corresponding covering is homotopy equivalent to the sphere.

4.2 Random points in higher dimension

The next example could not be done by computing the full Delaunay triangulation. We chose 1000 points in \mathbb{R}^{10} by selecting each coordinate uniformly at random from the interval $[-1, 1]$, producing a point cloud $S \subset \mathbb{R}^{10}$. We then com-

puted the alpha complex $X = \text{Alpha}(S, 1.0)$ up to the 3-simplices. The radius was such that the maximum degree in the Čech graph was about half the size of the data set, in our example 451. The full calculation took approximately 5 minutes, resulting in complex of sizes $(|X_k|)_{k=0}^3 = (1000, 64785, 560459, 1783194)$.

4.3 Two persistence examples

We next tested our algorithm on two well-studied data sets from persistent homology. Both are freely available online, and are explained in Henry Adams' tutorial on topological data analysis and Ripser [1]. We find that the first one, which is a 24-dimensional data set consisting of conformations of the cyclooctane molecule, is well-suited for the alpha complex because it tends to lie near the surface of a lower-dimensional space. The second one, which is a 9-dimensional database of optical image patches, leads to a complex with more simplices, because it has thickness in more dimensions, despite being embedded in lower dimensions.

Our first example is a data set consisting of 6040 points $S \subset \mathbb{R}^{24}$ in 24 dimensions, which correspond to conformations of the cyclooctane molecule, introduced in [31]. The authors found that the set of conformations tend to lie on a 2-dimensional topological subspace X which is an interesting union of a Klein bottle and a sphere. Because of its interesting topological type, it is a well-suited use case of persistent homology, in particular Ripser. By running Ripser on the full data set up to a cutoff distance of .5, we obtain a diagram of persistence intervals as shown in Figure 5, which agrees with the desired Betti numbers of $(\beta_k(X))_{k=0}^2 = (1, 1, 2)$. Ripser took approximately 48 seconds to complete this calculation.

We then computed the alpha complex $\text{Alpha}(S, .25)$ up the 3-simplices, as required to compute up to the second Betti number. Notice that our cutoff of $a_1 = .25$ is half the cutoff used for Ripser, because the minimum radius at which two balls intersect is half the distance between the centers. This computation took approximately 7 seconds, producing a complex of sizes $(|X_k|)_{k=0}^3 = (6040, 24646, 28352, 11858)$. We checked that it produced the desired Betti numbers exactly, without any persistence. Despite the much smaller size of the alpha complex as compared with the Vietoris-Rips construction, our homology calculation took longer, as we made no effort to use specialized algorithms.

We then applied the same procedure to a nine-dimensional data set studied in [27], consisting of normalized 3×3 patches taken from the van Hateren and van er Shaaf image database [42]. Certain high-density subsets were studied using persistent homology in [23], revealing the topological type of certain subspaces of a parametrized Klein bottle. We apply our algorithm to a subset $S \subset \mathbb{R}^9$ of size 1000 which is known to have the topological type of a circle, and which is denoted $X(300, 30)$ in [23]. We computed $\text{Alpha}(S, .5)$ up to the 2-dimensional simplices, obtaining a complex of sizes $(|X_k|)_{k=0}^2 = (1000, 44080, 454843)$ in about 38 seconds, and computed Betti numbers of $(1, 1)$, which agree with those of the circle. In this example, Ripser took only 1.5 seconds to obtain persistence intervals indicating these numbers.

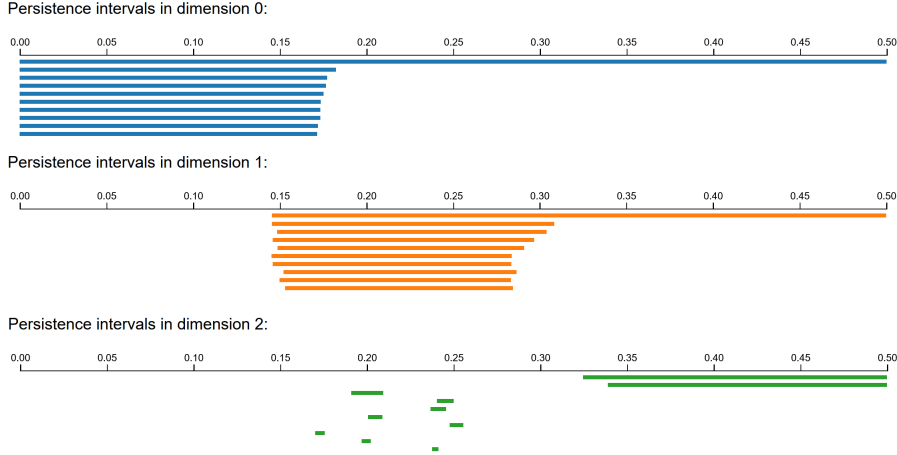


Figure 5: Persistence intervals of the cyclooctane data set as computed by Ripser. Many intervals not shown for viewability.

4.4 Spherical images from different angles

We next consider the alpha complex of a data set consisting of 28×28 color images of a coloring of the surface of the sphere from different angles, viewed as vectors in dimension $28 \times 28 \times 3$. This example could not be accomplished using an algorithm that begins by computing the full Delaunay triangulation due to the prohibitively high dimension. This illustrates a point that in dual programming the high dimensionality of the ambient space is not a direct factor as the input is a function only of respective dot products. Indeed, the only part of Algorithm 1 that depends explicitly on the dimension is line 11, in which the coefficients of the quadratic program are computed, which only happens once per vertex in each dimension.

Fix a function $\varphi : S^2 \rightarrow \mathbb{R}^3$ thought of as a coloring of the surface of a sphere. We will be interested in the following two choices:

$$\varphi_1(x, y, z) = (x, y, z), \quad \varphi_2(x, y, z) = (tx, ty, tz)$$

where $t = \max(z, 0)$, so that one hemisphere is sent to the origin. We then have a map $F_\varphi : SO(3) \rightarrow \mathbb{R}^m$ for $m = 28 \cdot 28 \cdot 3$ defined by projecting $\varphi \circ R^{-1}$ onto the xy -plane and discretizing the result into a 28×28 image. In other words, we take an image using a camera with position defined by R with no perspective warping. A collection of these images are shown in Figure 6.

For $\varphi = \varphi_1$, we randomly generated $N = 1000000$ images, producing a point cloud $D \subset \mathbb{R}^m$. We then selected landmarks $S \subset X$, until every element of D was within a distance of 8.0 of some element of S , giving a size of $|S| = 809$. Assuming that a covering by balls of radius 10.0 with centers at the points of S would cover the entire image of F_{φ_1} , we proceeded to compute $X = \text{Alpha}(S, 10.0)$ up to the 4-simplices. The resulting complex took

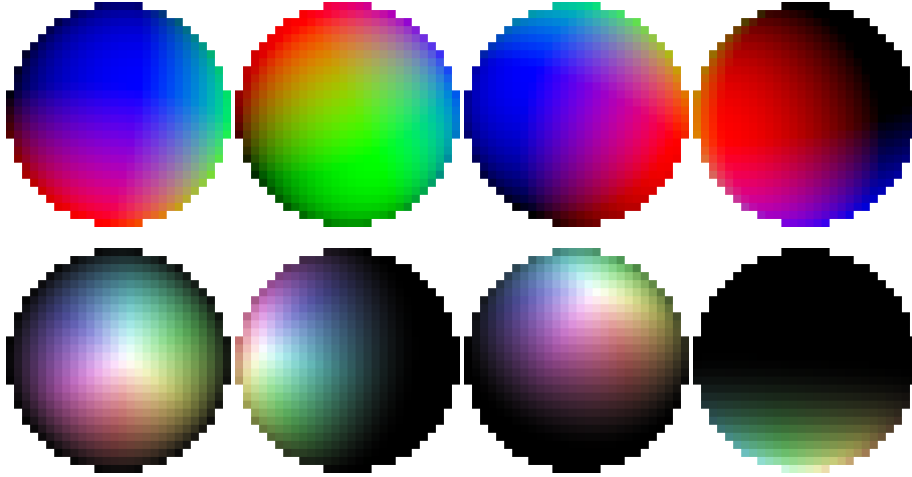


Figure 6: Top row: Pictures of a sphere from colored by φ_1 from different angles, corresponding the RGB values with the three axes. Bottom row: The same for φ_2 , displayed using a cylindrical HSV coloring scheme.

approximately 20 seconds in each dimension, and had sizes of

$$(|X_k|)_{k=0}^4 = (809, 7717, 17694, 15490, 5599),$$

We then computed the Betti numbers up to dimension 3 over the fields $\mathbb{F}_2, \mathbb{F}_3$, giving

$$(\beta_k(X, \mathbb{F}_2)) = (1, 1, 1, 1), \quad (\beta_k(X, \mathbb{F}_3)) = (1, 0, 0, 1).$$

These are the desired Betti numbers of $SO(3) \cong \mathbb{RP}^3$, which is to be expected if F_{φ_1} is a reasonable embedding of $SO(3)$ in \mathbb{R}^m .

We then performed a similar calculation for $\varphi = \varphi_2$. Since distances are smaller for this embedding, we used a minimum distance of 3.0 in selecting the landmark points, yielding a set S of size 2361. We then computed $\text{Alpha}(S, 3.5)$ up to the 4-simplices, which took approximately fifteen minutes, yielding a complex of X with sizes

$$(|X_k|)_{k=0}^4 = (2340, 24463, 68150, 102772, 128302).$$

We first notice that the number of simplices increases more rapidly with degree, whereas the one from the previous paragraph began to decrease above the 2-simplices. This is because the image $F_{\varphi_2}(SO(3))$ is pinched at the angle which is entirely on the dark side, resulting in a higher-dimensional tangent space. This makes the alpha complex effectively four-dimensional nearby the singularity. For instance, a single vertex corresponding to a nearly entirely black image had $(1, 105, 1756, 11776, 39376)$ simplices in each degree containing it as a face.

The Betti numbers were the calculated as above, yielding

$$(\beta_k(X, \mathbb{F}_p)) = (1, 0, 1, 1)$$

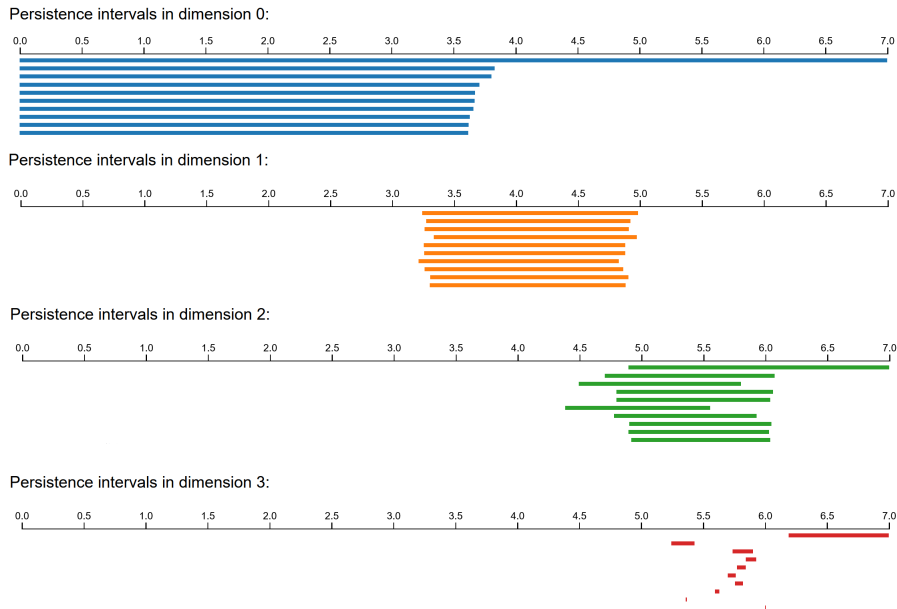


Figure 7: Results of Applying Ripser to samples from the data set of spherical images with one side colored entirely black. The intervals which extend to the rightmost endpoint indicate Betti numbers of $(1, 0, 1, 1)$.

for all primes p . In fact, these are the desired Betti numbers resulting from collapsing the circle $S^1 \subset SO(3)$ to a point, where the circle is the stabilizer of the image that is completely on the dark side of the coloring. This agrees with what may be computed using the long exact sequence for relative homology groups $H_k(SO(3), S^1)$. In the case of $p = 2$, we must use the fact that the map $H_1(S^1, \mathbb{F}_2) \rightarrow H_1(SO(3), \mathbb{F}_2)$ is nonzero, so that the connecting homomorphism is trivial. This results from the fact that S^1 corresponds to a generator of the fundamental group $\pi_1(SO(3)) = \mathbb{Z}_2$.

We then uploaded the second example into Ripser up to a distance cutoff of 7.0. The results, which took approximately 30 seconds to compute, are shown in Figure 7.

4.5 Homology groups of configuration spaces

In the next example, we use the alpha complex to carry out a complex homology calculation, which is the homology groups of a compact form of the ordered configuration space $\text{Conf}_n(\mathbb{R}^2)$ of n -points in the plane for $n = 3, 4$. Additionally, $\text{Conf}_n(\mathbb{R}^2)$ is acted on freely by the symmetric group S_n by relabeling, which induces an action on homology. By selecting landmark points in symmetric way, we generalize the Betti number computation and produce the decomposition

into irreducible characters of the corresponding group representation, which is an interesting object in geometric representation theory. This makes use of the theoretically sound nature of the alpha complex, which computes homology exactly.

Let $\text{Conf}_n(M)$ denote the configuration space of n points in M

$$\text{Conf}_n(M) = \{(x_1, \dots, x_n) \in M^n : x_i \neq x_j \text{ for all } i \neq j\}.$$

Its homology and cohomology have been well-studied, see [11]. Of particular interest is in the case of $\text{Conf}_n(\mathbb{R}^2)$, in which case the cohomology groups are the same as the cohomology of the pure Artin Braid group [41]. The Betti numbers are given in characteristic zero in this case by the formula

$$\sum_{k \geq 0} (-t)^k \beta_k(\text{Conf}_n(\mathbb{R}^2), \mathbb{Q}) = (1-t)(1-2t) \cdots (1-(n-1)t). \quad (14)$$

For instance, the first three Betti numbers of $\text{Conf}_3(\mathbb{R}^2)$ would be $(1, 3, 2)$ with all higher Betti numbers being zero, and would be $(1, 6, 11, 6)$ in the case of $n = 4$. These numbers are known as Stirling numbers of the first kind.

We also the action of the symmetric group by reordering the labels of the points,

$$\sigma \cdot (x_1, \dots, x_n) = (x_{\sigma_1}, \dots, x_{\sigma_n}).$$

The induced action makes both homology and cohomology into representations of the symmetric group. They turn out to be graded versions of the regular representation after twisting by the sign representation in odd degree, noticing that the above total dimensions from the previous paragraph sum to $n!$. A formula for the character of this action over complex coefficients is a special case of a results of Lehrer and Solomon [28]. In this case, it says that the trace of the action of a permutation σ on cohomology is given by

$$\sum_i (-t)^i \text{Tr}(\sigma, H^i(\text{Conf}_n(\mathbb{R}^2), \mathbb{C})) = t^n \prod_{i=1}^{\infty} \prod_{j=1}^{m_i(\lambda)} (\alpha_i(t^{-1}) - (j-1)i) \quad (15)$$

where $\lambda = (\lambda_1, \dots, \lambda_l)$ is a Young diagram describing the cycle type of σ , $m_i(\lambda)$ is the number of times that each i appears in the elements of λ , and

$$\alpha_j(t) = \sum_{d|j} t^d \mu(j/d)$$

where μ is the usual Möbius function. In particular, we recover formula (14) by taking σ to be the identity permutation.

A priori, $\text{Conf}_n(\mathbb{R}^2)$ is not well-suited to being triangulated because the constraint that $x_i \neq x_j$ is of measure zero, and so would not be detected by distance measurements. We will instead replace the full configuration space with the compact subspace $C_n \subset \text{Conf}_n(\mathbb{R}^2)$, which consists of all points $(x_1, \dots, x_n) \in \mathbb{R}^2$ satisfying:

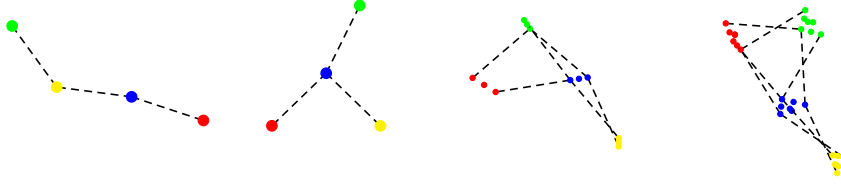


Figure 8: On the left, two typical points in C_4 , one with each of the two types of associated tree structure describing which points are separated by distance exactly 1. On the right, the endpoints of the Barycentric subdivision of simplices of the resulting alpha complex $X^{(4)}$ of dimensions 1 and 2, embedded using the witness map Φ . Notice that simplices may connect vertices with different associated graphs G .

- The points are mean centered, i.e. $x_1 + \dots + x_n = (0, 0)$.
- For every $i \neq j$, we have that $\|x_i - x_j\| \geq 1$.
- The graph G on n vertices which contains an edge connecting i and j whenever we have equality $\|x_i - x_j\| = 1$ is connected.

We illustrate some typical points in Figure 8, showing the graph G in dashed lines, which is generically a tree. While $\text{Conf}_n(\mathbb{R}^2)$ is smooth but not compact of dimension $2n$, it is not hard to see that C_n is singular but compact of dimension $n - 1$. We also observe that C_n is preserved by the S_n action on $\text{Conf}_n(M)$.

In a similar way as previous example, we selected landmark points $S^{(n)}$ from C_n for the values of $n = 3, 4$, using a distance cutoff of .3 in both cases. In order to maintain an S_n -action on the complex itself, we sampled in such a way that whenever a single point is added to, we also added its S_n -orbit. The resulting sizes were $|S^{(3)}| = 328$, $|S^{(4)}| = 20232$, noticing that the sizes are multiples of 6 and 24 respectively.

We first attempted to compute the homology groups using Ripser, by uploading $S^{(n)}$ to the Ripser live, with a cutoff distance of .7, which more than the lower bound of .6 for the distance between any two points. Not surprisingly, the case of $n = 3$ was trivial. Ripser was able to compute the homology groups up to the second Betti number for $S^{(4)}$ in 30-40 minutes, though did not manage to compute the third Betti number. The results are shown in Figure 9.

We then computed the full alpha complexes to top dimension, with a distance cutoff of .35, yielding filtered complexes $X^{(n)} = \text{Alpha}(S^{(n)}, .35, 4)$. The first one $X^{(3)}$ took under one second to compute, whereas computing $X^{(4)}$ took approximately 4 minutes. The resulting sizes were

$$\begin{aligned} (|X^{(3)}|)_{k=0}^4 &= (328, 1245, 1201, 312, 28), \\ (|X^{(4)}|)_{k=0}^4 &= (20232, 228072, 608928, 665208, 345888, 92040, 10272), \end{aligned} \quad (16)$$

all others sizes being empty because the spaces are embedded into dimension $2n - 2$ by the mean-centering condition. Notice that the Euler characteristics

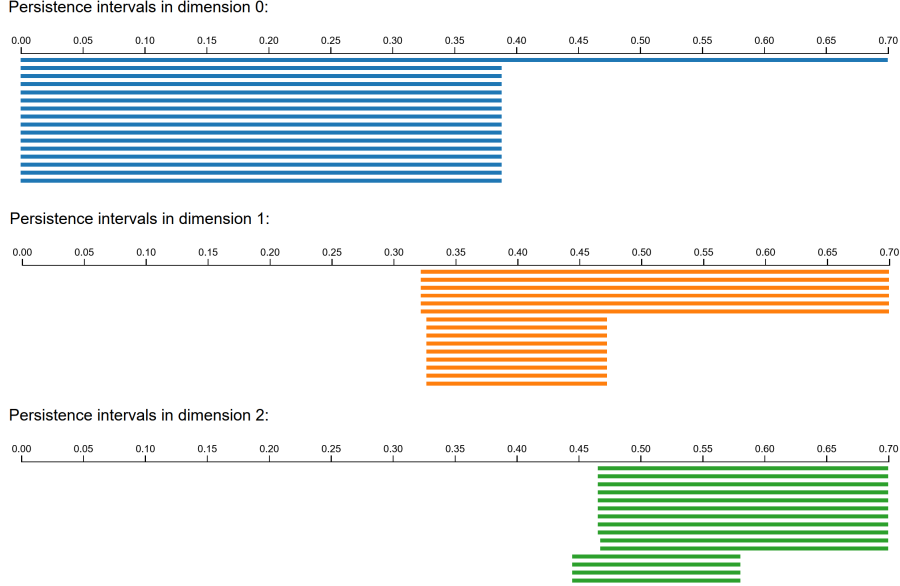


Figure 9: Results of Applying Ripser to samples from the configuration space C_4 , with a very large number of shorter length persistence intervals excluded for viewability. We see the first three Betti numbers of $(1, 6, 11)$.

are zero, and that each number is a multiple of $n!$. Some typical two and three-simplices are shown on the right side of Figure 8. By the way we chose the landmark points, we have an action of the symmetric group on each $X_k^{(n)}$, and that the boundary maps commute with this action.

The two spaces had Betti numbers that agreed with (14). To compute the character of the S_n -representation, we applied Mashke's theorem to convert the boundary operator $\partial_k : C_k(X^{(n)}, \mathbb{F}_5) \rightarrow C_{k-1}(X^{(n)}, \mathbb{F}_5)$ into block-diagonal form, with one component for each irreducible representation of S_n , noting that the coefficient field \mathbb{F}_p satisfies $p > n$. The homology computation took very long for the $n = 4$ case, several hours for each block in each dimension, though this could be made much more efficient by incorporating group actions into state of the art methods for homology calculations. We found for $n = 4$ that

$$\sum_{k=0}^4 (-t)^k \text{ch } H_k(X^{(4)}, \mathbb{F}_5) = \chi_{(4)} - (\chi_4 + \chi_{3,1} + \chi_{2,2})t + (2\chi_{3,1} + \chi_{2,2} + \chi_{2,1,1})t^2 - (\chi_{3,1} + \chi_{2,1,1})t^3,$$

where χ_λ denotes the irreducible character of S_4 for a given Young diagram λ . This agrees with the predicted value for the full space $\text{Conf}_n(\mathbb{R}^2)$ that one would obtain from equation (15). Replacing each irreducible character with

their corresponding dimensions

$$(\chi_4, \chi_{3,1}, \chi_{2,2}, \chi_{2,1,1}, \chi_{1,1,1,1}) \mapsto (1, 3, 2, 3, 1),$$

we recover the expected value of $1 - 6t + 11t^2 - 6t^3$.

References

- [1] Henry Adams. Tutorial on topological data analysis. <https://github.com/ds4m/topological-data-analysis/wiki>.
- [2] Daniel Arnström, Alberto Bemporad, and Daniel Axehill. A dual active-set solver for embedded quadratic programming using recursive ldl^T updates. *IEEE Transactions on Automatic Control*, 67(8):4362–4369, 2022.
- [3] F. Aurenhammer and H. Edelsbrunner. An optimal algorithm for constructing the weighted voronoi diagram in the plane. *Pattern Recognition*, 17(2):251–257, 1984.
- [4] C.B. Barber, D.P. Dobkin, and H.T. Huhdanpaa. The quickhull algorithm for convex hulls. *ACM Trans. on Mathematical Software*, 22(4):469–483, 1996.
- [5] Ulrich Bauer. Ripser: efficient computation of Vietoris-Rips persistence barcodes. *J. Appl. Comput. Topol.*, 5(3):391–423, 2021.
- [6] Ulrich Bauer and Herbert Edelsbrunner. The morse theory of Čech and delaunay filtrations. In *Proceedings of the Thirtieth Annual Symposium on Computational Geometry*, SOCG’14, page 484–490, New York, NY, USA, 2014. Association for Computing Machinery.
- [7] Ulrich Bauer, Michael Kerber, Fabian Roll, and Alexander Rolle. A unified view on the functorial nerve theorem and its variations. *Expositiones Mathematicae*, 2023.
- [8] Prosenjit Bose, Anna Lubiw, Vinayak Pathak, and Sander Verdonschot. Flipping edge-labelled triangulations. *Computational Geometry*, 68:309–326, 2018. Special Issue in Memory of Ferran Hurtado.
- [9] Adrian Bowyer. Computing dirichlet tessellations. *Comput. J.*, 24:162–166, 1981.
- [10] Erik Carlsson and John Carlsson. A witness complex for density landscapes, 2023.
- [11] F.R. Cohen. On configuration spaces, their homology, and lie algebras. *Journal of Pure and Applied Algebra*, 100(1):19–42, 1995.

- [12] Tran Kai Frank Da, Sébastien Lorient, and Mariette Yvinec. 3D alpha shapes. In *CGAL User and Reference Manual*. CGAL Editorial Board, 5.5.2 edition, 2023.
- [13] P.A. De-Alarcon, A.P. Pascual-Montano, A. Gupta, and J.M. Carazo. Modeling shape and topology of 3d images of biological specimens. In *2002 International Conference on Pattern Recognition*, volume 1, pages 79–82 vol.1, 2002.
- [14] Vin de Silva. A weak characterisation of the delaunay triangulation. *geom. dedic.* 135(1), 39-64. *Geom. Dedicata*, 135:39–64, 08 2008.
- [15] Jean-Guillaume Dumas and Gilles Villard. Computing the rank of large sparse matrices over finite fields. *Computer Algebra in Scientific Computing (CASC)*, pages 47–62, 2002.
- [16] Edelsbrunner, Letscher, and Zomorodian. Topological persistence and simplification. *Discrete & Computational Geometry*, 28:511–533, 2002.
- [17] H. Edelsbrunner and E. Mücke. Three-dimensional alpha shapes. *ACM Trans. Graph.*, 13(1), 1994.
- [18] H. Edelsbrunner, University of Illinois at Urbana-Champaign. Department of Computer Science, and N.R. Shah. *Incremental Topological Flipping Works for Regular Triangulations*. Report (University of Illinois at Urbana-Champaign. Department of Computer Science). University of Illinois at Urbana-Champaign, Department of Computer Science, 1992.
- [19] Herbert Edelsbrunner. Weighted alpha shapes. In *Rept. UIUCDCS-R-92-1760, Dept. Comput. Sci., Univ. Illinois at Urbana-Champaign, Illinois*, 1992.
- [20] Herbert Edelsbrunner. *Surface Reconstruction by Wrapping Finite Sets in Space*, pages 379–404. Springer Berlin Heidelberg, Berlin, Heidelberg, 2003.
- [21] Herbert Edelsbrunner and John Harer. *Computational Topology - an Introduction*. American Mathematical Society, 2010.
- [22] Herbert Edelsbrunner and Raimund Seidel. Voronoi diagrams and arrangements. In *Proceedings of the First Annual Symposium on Computational Geometry*, SCG '85, page 251–262, New York, NY, USA, 1985. Association for Computing Machinery.
- [23] Carlsson G., T. Ishkhanov, V. de Silva, and A. Zomorodian. On the local behavior of spaces of natural images. *Int J Comput Vis*, 76:1–12, 2008.
- [24] Jean-Claude Hausmann. On the vietoris-rips complexes and a cohomology theory for metric spaces. *Annals of Mathematics Studies*, 138:175–188, 1995.

- [25] F. Hurtado, M. Noy, and J. Urrutia. Flipping edges in triangulations. In *Proceedings of the Twelfth Annual Symposium on Computational Geometry*, SCG '96, page 214–223, New York, NY, USA, 1996. Association for Computing Machinery.
- [26] Rolf Klein, Kurt Mehlhorn, and Stefan Meiser. Randomized incremental construction of abstract voronoi diagrams. *Computational Geometry*, 3(3):157–184, 1993.
- [27] Ann B. Lee, Kim S. Pedersen, and David Mumford. The nonlinear statistics of high-contrast patches in natural images. *International Journal of Computer Vision*, 54:83–103, 2003.
- [28] G. I. Lehrer and Louis Solomon. On the action of the symmetric group on the cohomology of the complement of its reflecting hyperplanes. *Journal of Algebra*, 104:410–424, 1986.
- [29] Jean-L. Leray. L’anneau spectral et l’anneau filtré d’homologie d’un espace localement compact et d’une application continue. *J. Math. Pures Appl*, 9, 1950.
- [30] Jie Liang, Herbert Edelsbrunner, Ping Fu, Pamidighantam V Sudhakar, and Shankar Subramaniam. Analytical shape computation of macromolecules: I. molecular area and volume through alpha shape. *Proteins: Structure, Function, and Bioinformatics*, 33(1):1–17, 1998.
- [31] S. Martin, A. Thompson, E.A. Coutsiias, and J.P. Watson. Topology of cyclo-octane energy landscape. *J Chem Phys.*, 23, 2010.
- [32] Amish Mishra and Francis Motta. Stability and machine learning applications of persistent homology using the delaunay-rips complex. *Front. Appl. Math. Stat.*, 9, 2023.
- [33] Nina Otter, Mason Porter, Ulrike Tillmann, Peter Grindrod, and Heather Harrington. A roadmap for the computation of persistent homology. *EPJ Data Science*, 6, 06 2015.
- [34] Donald R. Sheehy. An output-sensitive algorithm for computing weighted α -complexes. In *Proceedings of the 27th Canadian Conference on Computational Geometry, CCCG 2015, Kingston, Ontario, Canada, August 10-12, 2015*. Queen’s University, Ontario, Canada, 2015.
- [35] Vin de Silva and Gunnar Carlsson. Topological estimation using witness complexes. In Markus Gross, Hanspeter Pfister, Marc Alexa, and Szymon Rusinkiewicz, editors, *SPBG'04 Symposium on Point - Based Graphics 2004*. The Eurographics Association, 2004.
- [36] E.V. Somasundaram, S.E. Brown, A. Litzler, J.G. Scott, and R.R. Wadhwa. Benchmarking r packages for calculation of persistent homology. *R Journal*, 13(1), 2020.

- [37] Alexander Stukowski. Computational analysis methods in atomistic modeling of crystals. *Jom*, 66:399–407, 2014.
- [38] The CGAL Project. *CGAL User and Reference Manual*. CGAL Editorial Board, 5.5.2 edition, 2023.
- [39] Chris Tralie and Nathaniel Saul. Cechmate. Version 0.1. 0. url: <https://github.com/scikit-tda/cechmate>.
- [40] Greg Turk and Marc Levoy. Zippered polygon meshes from range images. *Proceedings of the 21st annual conference on Computer graphics and interactive techniques*, 1994.
- [41] F.V Vainshtein. Cohomology of the braid groups. *Func. Anal. Appl.*, 12, 1978.
- [42] van Hateren J.H and A_z van der Schaaf. Independent component filters of natural images compared with simple cells in primary visual cortex. *Proc. R. Soc. Lond. B*, pages 359–366, 1998.
- [43] D. F. Watson. Computing the n-dimensional Delaunay tessellation with application to Voronoi polytopes*. *The Computer Journal*, 24(2):167–172, 01 1981.
- [44] Afra Zomorodian and Gunnar Carlsson. Computing persistent homology. In *Proceedings of the twentieth annual symposium on Computational geometry*, pages 347–356, 2004.